# Au Nanomatryoshkas as Efficient Near-Infrared Photothermal Transducers for Cancer Treatment: Benchmarking against Nanoshells

Ciceron Ayala-Orozco,[†,∥] Cordula Urban,[‡,∥] Mark W. Knight,[§] Alexander Skyrme Urban,[§] Oara Neumann,[§] Sandra W. Bishnoi,[§] Shaunak Mukherjee,[†] Amanda M. Goodman,[†] Heather Charron,[‡] Tamika Mitchell,[⊥] Martin Shea,[⊥] Ronita Roy,[‡] Sarmistha Nanda,[⊥] Rachel Schiff,[⊥] Naomi J. Halas,[†,§,*] and Amit Joshi[‡,*]

[†]Department of Chemistry, Rice University, 6100 Main Street, Houston, Texas 77005, United States, [‡]Division of Molecular Imaging, Department of Radiology, Baylor College of Medicine, BCM 360, One Baylor Plaza, Houston, Texas 77030, United States, [§]Department of Electrical and Computer Engineering, Rice University, 6100 Main Street, Houston, Texas 77005, United States, and [⊥]Lester and Sue Smith Breast Center, Baylor College of Medicine, Houston, Texas 77030, United States. [∥]C. Ayala-Orozco and C. Urban contributed equally.

**ABSTRACT** Au nanoparticles with plasmon resonances in the near-infrared (NIR) region of the spectrum efficiently convert light into heat, a property useful for the photothermal ablation of cancerous tumors subsequent to nanoparticle uptake at the tumor site. A critical aspect of this process is nanoparticle size, which influences both tumor uptake and photothermal efficiency. Here, we report a direct comparative study of ∼90 nm diameter Au nanomatryoshkas ($Au/SiO_2/Au$) and ∼150 nm diameter Au nanoshells for photothermal therapeutic efficacy in highly aggressive triple negative breast cancer (TNBC) tumors in mice. Au nanomatryoshkas are strong light absorbers with 77% absorption efficiency, while the nanoshells are weaker absorbers with only 15% absorption efficiency. After an intravenous injection of Au nanomatryoshkas followed by a single NIR laser dose of 2 W/cm$^2$ for 5 min, 83% of the TNBC tumor-bearing mice appeared healthy and tumor free >60 days later, while only 33% of mice treated with nanoshells survived the same period. The smaller size and larger absorption cross section of Au nanomatryoshkas combine to make this nanoparticle more effective than Au nanoshells for photothermal cancer therapy.
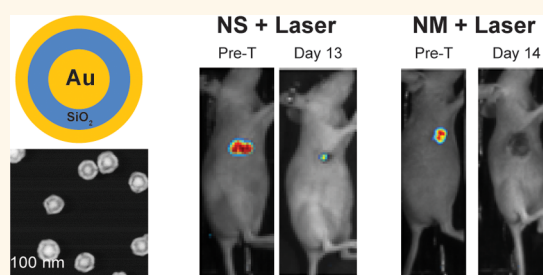
**KEYWORDS:** nanomatryoshka · multilayer nanoshells $Au/SiO_2/Au$ · photothermal therapy · near-infrared · Au nanoparticle

Nanoparticle-mediated photothermal ablation of tumors with near-infrared (NIR) light is an emerging tool in the fight against cancer. Unlike conventional approaches to treatment, such as surgery, radiation therapy, and chemotherapy, nanoparticle treatments are minimally invasive, can be passive or targeted, and should result in minimal side effects.[1−8] In photothermal therapy, light is administered, absorbed by the particles and converted into heat sufficient to destroy cells in the local vicinity of the nanoparticle. The treatment is performed with laser light at NIR wavelengths (∼800 nm), where the penetration depth of light in biological tissue is maximum (therapeutic window).[9] NIR absorbing Au-based nanoparticles serving as photothermal transducers are the key components

for this treatment. Since the first demonstration of Au nanoshells as NIR photothermal transducers,[1] many other nanoparticles such as Au nanorods,[4] nanocages,[7] hollow Au nanoshells,[5] carbon nanotubes,[6] and graphene[8] have also been actively investigated for photothermal tumor ablation. All these photothermal transducers provide a wide range of geometries with various compositions and therefore different capabilities, advantages and limitations in photothermal therapy.

An ideal nanoparticle photothermal transducer should have the following features: (1) NIR absorption between 700−1000 nm, (2) a large absorption cross-section, (3) a size below 100 nm to enhance tumor uptake and to reduce sequestration by the reticuloendothelial system (RES), and (4) low

toxicity and biocompatibility of chemical components. Au nanoparticles absorbing in the NIR have been shown to be excellent photothermal transducers due to their plasmon resonance,[1,7,10] the collective oscillation of conduction electrons that occurs upon optical excitation at the resonance frequency of the nanoparticle. Plasmon resonance frequencies can be tuned to the NIR therapeutic window by controlling the geometry and size of the Au nanoparticles.[11] Au is also a particularly attractive material because of its biocompatibility and low cytotoxicity.

Among Au plasmonic nanoparticles, nanoshells can sustain large absorption cross sections due to their spherical geometry, thereby providing high photothermal conversion efficiencies.[10] Additional advantages of Au nanoshells over other NIR absorbing gold nanoparticles are the noncytotoxicity and biocompatibility of their component materials, properties that have led to their current use in clinical trials.[12] In contrast, Au nanorods also offer NIR plasmon resonances with sizes in the sub-50 nm range; however, they are synthesized using high concentrations of cytotoxic cetyltrimethylammonium (CTAB) as a surfactant. Unfortunately, when CTAB is removed, the result is often a reshaping and/or an irreversible aggregation of the nanorods. Shape-preserving chemical functionalization strategies of nanorods are now available that limit the cytotoxicity of CTAB in vitro, but often they require multiple washing steps and are not suitable for long-term storage at physiological conditions.[13,14] In addition, strategies that provide replacement of CTAB with cationic thiol functionalities still have not been evaluated for their in vivo biodistribution, but it is likely that due to their high positive charge that they will have shorter circulation half lives than PEGylated nanoparticles.[15]

Au nanocages and hollow Au nanoshells (HGNS) are synthesized using a galvanic replacement reaction consisting of Au reduction on a sacrificial metallic core of Ag or Co through a redox process.[13−16] In this reaction, residual Ag and Co can remain inside of, or alloyed with, the hollow Au nanostructures, raising potential in vivo stability and cytotoxicity issues.[17−20] Therefore, $SiO_2$/Au nanoshells remain as one of the most promising systems for photothermal therapy.[2,21,22] Unfortunately, current experimental synthesis limits NIR absorbing $SiO_2$/Au nanoshells to diameters above 100 nm. The development of directly clinically translatable NIR-absorbing sub-100 nm Au nanoparticles remains an important challenge.

Multilayered Au nanoparticles (Au/$SiO_2$/Au), known as nanomatryoshkas, offer the possibility to achieve NIR plasmon resonances in the sub-100 nm size range.[7] Nanomatryoshkas (Au/$SiO_2$/Au) consist of a Au nanoparticle core, coated with a thin silica layer, surrounded by a final thin Au shell. Due to strong coupling between the plasmons supported by the Au core and the Au

shell, known as plasmon hybridization, the plasmon resonance can be tuned to the NIR region in particles with smaller overall dimensions than the standard $SiO_2$/Au nanoshell.[7] The development of sub-100 nm nanomatryoshkas is potentially a critical advancement in optimizing photothermal cancer therapy. However, the large scale synthesis required for this application has been hindered by the low efficiency of the amine functionalization of the synthetic precursor Au/$SiO_2$ nanoparticle prior to growth of the terminal Au layer of the nanoparticle.[7]

Here we report a direct comparative study of sub-100 nm Au nanomatryoshkas and ∼150 nm diameter Au nanoshells in photothermal cancer therapy. This study was facilitated by improvements to the nanomatryoshka synthesis which significantly increased nanoparticle yield, making in vivo studies possible. Here we demonstrate the first use of nanomatryoshkas as photothermal transducers in cancer studies in mice, for the therapy of highly aggressive triple negative breast cancer (TNBC) tumors. The subtype TNBC accounts for about 15% of breast cancer cases and is characterized by the lack of estrogen receptor, progesterone receptor, and epidermal growth factor receptor 2 (HER2).[23] Few therapeutic options currently exist for TNBC, a highly aggressive cancer associated with poor patient prognosis, shorter survival times, and nonresponsiveness to endocrine and immunotherapies.[23−25] A challenge for nanomedicine in the treatment of TNBC is the lack of traditional targeting receptors. For that reason, passive accumulation of particles in the tumor by the enhanced permeability and retention (EPR) effect is one of the primary mechanisms for nanoparticle intratumoral uptake. Since EPR-based nanoparticle accumulation in tumors strongly depends on nanoparticle size,[26,27] it is vitally important to obtain suitable candidate nanoparticles in the sub-100 nm size range. In this study, we show that sub-100 nm diameter Au nanomatryoshkas exhibit enhanced accumulation in tumors and improved photothermal conversion efficiency relative to a parallel treatment using Au nanoshells, conditions which resulted in a substantially higher survival rate of the nanomatryoshka treated mice.

## RESULTS AND DISCUSSION

**Synthesis and Characterization of Au Nanomatryoshkas and Au Nanoshells.** Au nanomatryoshkas were synthesized through an improved method of a previously reported protocol.[7] In the previous method, the first step involves coating the Au colloid with a uniform layer of $SiO_2$ and subsequent amine functionalization. Here a key improvement comes from doping the $SiO_2$ layer with (3-aminopropyl)triethoxysilane (APTES) during $SiO_2$ layer synthesis, which better facilitates binding of Au colloid (1−2 nm in diameter) onto the surface of the silica layer. The ultrasmall Au nanoparticles act as seeds for growth of the terminal Au shell layer,
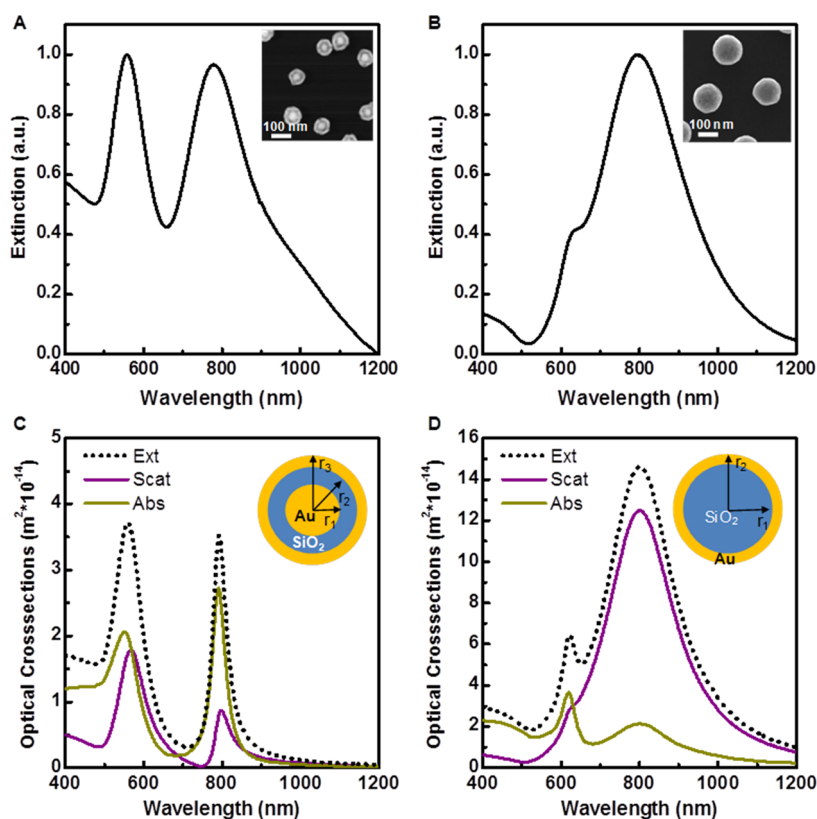
**Figure 1. Optical and structural properties of nanomatryoshkas and nanoshells. (A)** Experimental ensemble extinction spectrum of nanomatryoshkas (inset: SEM image of nanomatryoshkas with dimensions $[r_1, r_2, r_3]$ = [21, 31, 44] nm). **(B)** Experimental ensemble extinction spectrum of nanoshells (inset: SEM image of nanoshells with dimensions $[r_1, r_2]$ = [62, 76] nm). **(C)** Calculated extinction, scattering and absorption cross section spectra (Mie theory) of the $[r_1, r_2, r_3]$ = [21, 31, 44] nm nanomatryoshka. **(D)** Calculated extinction, scattering and absorption cross section spectra (Mie theory) of the $[r_1, r_2]$ = [62, 76] nanoshell.

completing the Au nanomatryoshka synthesis. The thickness of the silica layer is critical for obtaining a high degree of control over the hybridized plasmon resonance modes in nanomatryoshkas, essential for strong NIR absorption. This modified method allows precise control of the silica thickness by first growing an oversized silica layer (~16 nm) on the Au core followed by controlled etch-back of the silica layer by hydrolysis. (The etching process takes place during the incubation in the Duff colloid solution[28] as described in the fabrication of the seeded precursor in the Methods section.) In this step, the size of the silica layer was thinned to 10 nm after 4 days of incubation. During the etching process, the APTES-doped silica also became densely covered with (1−2 nm) Au nanoparticles, bound to the nitrogen of the amine group of the APTES. An outer shell of Au was synthesized around this seeded precursor by reducing Au$^{3+}$ with formaldehyde as a reducing agent. The silica core/Au shell nanoshells used in this study were synthesized by standard methods previously published.[29]

Plasmon resonances in both Au nanomatryoshkas and Au nanoshells are highly tunable by control of nanoparticle dimensions.[7,11] For nanomatryoshkas, increasing the Au core size, using a thinner silica layer,

and growing thinner Au shells result in a tuning of the plasmon to longer wavelengths. In particular, thinner silica layers increase the interaction between the core AuNP and Au shell, which strongly red-shifts the plasmon resonance. The Au nanomatryoshkas synthesized here show two plasmon modes: a low-energy plasmon subradiant mode at 783 nm and a high-energy superradiant plasmon mode at 560 nm. These modes are associated with the nanomatryoshka shown in the inset of Figure 1A with dimensions $[r_1, r_2, r_3]$ = [20.8 ± 2.6, 31.3 ± 2.1, 44 ± 2.6] nm (nominally $[r_1, r_2, r_3]$ = [21, 31, 44] nm). The radii of each layer were determined from particle size statistics obtained from scanning electron microscope (SEM) images of over 1000 Au core particles, 500 seeded precursors, and 400 nanomatryoshkas. These strongly hybridized modes resulting from the core−shell interaction allow the plasmon to be tuned to ~800 nm for nanoparticles with diameters in the sub-100 nm size regime. Similarly, Au nanoshells exhibit a dipole plasmon mode that can be tuned to the NIR region by increasing the silica (SiO$_2$) core size and growing thinner Au shells. Decreasing the shell thickness facilitates an interaction between the surface plasmons of the inner and outer layers of the metallic shell.[11] The extinction spectrum

of Au nanoshells with a plasmon resonance at 796 nm is shown in Figure 1B. In the inset of Figure 1B a representative SEM image of nanoshells with average dimensions $[r_1, r_2] = [62 \pm 6.7, 76 \pm 4.7]$ nm (nominally $[r_1, r_2] = [62, 76]$ nm) can be observed. These dimensions were calculated from particle size statistics obtained from SEM images of over 300 $SiO_2$ core particles and 300 nanoshells.

**Absorption Cross Sections.** The absorption cross section ($\sigma_a$) of the nanoparticle is the optical parameter that is directly relevant to photothermal heating efficiency. In contrast, the scattering cross section ($\sigma_s$) does not contribute to photothermal conversion. The absorption cross section is defined as the product of the geometric cross section area ($\sigma_g$) and the absorption efficiency ($Q_a$):

$$\sigma_a = \sigma_g Q_a \qquad (1)$$

and is therefore directly proportional to nanoparticle size. The absorption efficiency, the ratio of the absorption cross section over the geometric cross sectional area (and analogously the scattering and extinction efficiencies), can be calculated from Mie theory. Calculated spectra of the optical (absorption, scattering and extinction) cross sections of a nanomatryoshka and a nanoshell are shown in Figure 1C,D. The absorption cross section of the nanomatryoshka at the absorption maximum wavelength of 800 nm is $2.7 \times 10^{-14}$ m$^2$ with a geometric cross section of $6.3 \times 10^{-15}$ m$^2$. For nanoshells, the absorption cross section is $2.1 \times 10^{-14}$ m$^2$ with a geometric cross section of $1.7 \times 10^{-14}$ m$^2$. Even though the geometric cross section of a nanoshell is ~3 times larger than the nanomatryoshka, the absorption cross section in the nanomatryoshka is ~1.3 fold larger than a nanoshell. The absorption efficiency for a nanomatryoshka is 4.26, which corresponds to 77% of the total extinction efficiency of 5.53. These nanomatryoshkas show a scattering efficiency of 1.26, 23% of their extinction efficiency. For nanoshells, the major contribution to the total extinction comes from a scattering efficiency of 7.25, which represents 85% of the extinction efficiency, with a minor contribution from the absorption efficiency of 1.24, only 15% of the total extinction efficiency. The larger absorption efficiency and smaller scattering efficiency of nanomatryoshkas will result in a higher photothermal transduction efficiency than that of the larger-diameter nanoshells.

**Photothermal Transduction Efficiency.** Photothermal transduction efficiency is a measure of how efficient a nanoparticle is in converting absorbed light into a temperature increase of its surroundings. To experimentally determine the photothermal transduction efficiencies of nanoshells and nanomatryoshkas, the temperature of each nanoparticle solution was measured while irradiated with an 810 nm laser until it reached equilibrium (Figure 2A). The optical density was maintained at 1.0 for both types of nanoparticles.
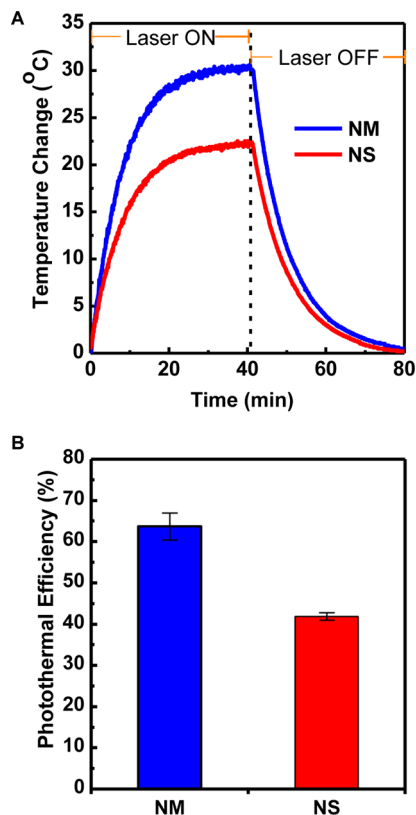


**Figure 2. Photothermal transduction of nanomatryoshkas and nanoshells. (A)** Temperature change in solutions of nanomatryoshkas and nanoshells (optical density = 1) irradiated 40 min with a laser of wavelength at 810 nm and power of 2 W/cm$^2$. **(B)** Mean photothermal efficiency from the conversion of light to heat in nanomatryoshka and nanoshell solutions (OD = 1).

This optical density corresponds to a concentration of $6.5 \times 10^9$ particles/mL for nanomatryoshkas and $1.6 \times 10^9$ particles/mL for nanoshells. Equal optical densities is the standard method for comparing photothermal efficiencies, since at equal nanoparticle concentrations, nanoshells will have a larger total geometric cross section than nanomatryoshkas.[10,30,31] The photothermal transduction efficiency ($\eta$) can be determined by[30]

$$\eta = \frac{hA(T_{max} - T_{amb}) - Q_0}{I(1 - 10^{-A_\lambda})} \qquad (2)$$

where $h$ is the heat transfer coefficient, $A$ is the sample well surface area, $T_{max}$ is the steady state maximum temperature, $T_{amb}$ is the ambient room temperature, $Q_0$ is the baseline energy input by the solvent and the sample cell without nanoparticles, $I$ is the laser power, and $A_\lambda$ is the optical density of the nanoparticle solution at the laser wavelength. The heating and cooling temperature data shown in Figure 2A have a characteristic thermal time constant:

$$\tau = \frac{\sum_i m_i C_{p,i}}{hA} \qquad (3)$$

where $m$ is the mass and $C_p$ is the heat capacity of each $i$ component of the sample cell. The mass of the

nanoparticle solution was 3.5 g, and its heat capacity ($C_{p,s}$) was approximated to be 4.187 J g$^{-1}$ K$^{-1}$ (the heat capacity of water). In addition, the mass of the quartz cuvette was 5.67 g, and its heat capacity ($C_{p,c}$) was 0.839 J g$^{-1}$ K$^{-1}$. By finding the best exponential fit of the cooling temperature data, we calculated the thermal time constant ($\tau$) using

$$T_{max} - T_{amb} = e^{-t/\tau} \tag{4}$$

The thermal time constant should be the same for either heating or cooling of the solution. Once we know the time constant we can calculate the heat transfer coefficient ($h$). The heat energy ($Q_0$) of the sample cell and solvent without nanoparticles was calculated similarly by calculating first the heat transfer coefficient from an independent experiment, and then using the following equation:

$$Q_0 = hA(T_{max} - T_{amb}) \tag{5}$$

The calculated photothermal transduction efficiency shows that the nanomatryoshkas have a higher average efficiency (63%) than nanoshells (39%) as shown in Figure 2B, in agreement with previously calculated values for nanoshells.[10] This indicates that nanomatryoshkas are 1.6 times more efficient than nanoshells at constant optical density of 1.0 for both nanoparticle systems.

**Biodistribution of Nanomatryoshkas and Nanoshells.** Nanomatryoshkas and nanoshells were functionalized with thiolated poly(ethylene glycol) (thiol-PEG) of molecular weight 10 kDa to render the nanoparticle surface biocompatible and to increase the circulation time in the bloodstream of the mice. The hydrodynamic diameter and surface charge of the PEG conjugated and nonconjugated particles are shown in Table 1. The surface charge is about −5 mV for PEG functionalized nanomatryoshkas and nanoshells. A close to neutral surface charge is required for longer circulation time in the bloodstream, better tumor penetration and evasion of the RES.[32,33]

PEG-conjugated nanomatryoshkas and nanoshells with an equal dose of gold (300 $\mu$g of Au) were delivered *via* tail vein injection into mice bearing a TNBC xenograft. This dose of Au is equivalent to $5.7 \times 10^{10}$ nanomatryoshkas in 200 $\mu$L (approximate OD$_{810\ nm}$ = 26) with dimensions $[r_1, r_2, r_3] = [21, 31, 44]$ nm and $1.9 \times 10^{10}$ nanoshells in 200 $\mu$L (approximate OD$_{810\ nm}$ = 42) with dimensions $[r_1, r_2] = [62, 76]$ nm considering that the density of gold is 19.3 g/cm$^3$. After the nanoparticles had circulated in the bloodstream, the mice were sacrificed at 4, 24, and 72 h postinjection and the Au content in each tumor was quantified using ICP-MS. The Au content in the mouse organs is shown in Figure 3. The circulation half-life of both nanoparticles is expected to be similar since no statistical difference was observed in the gold concentration in the blood at the time-points analyzed. For nanoshells previous studies have reported

**TABLE 1. Diameter and Surface Charge of PEG-Functionalized and Bare Gold Nanoparticles**

| sample | diameter SEM (nm) | hydrodynamic diameter (nm) | zeta potential (mV) |
|--------|-------------------|----------------------------|---------------------|
| NM | 88 ± 5 | 96 | −46.7 |
| NM@PEG | NA | 137 | −4.4 |
| NS | 152 ± 9 | 161 | −57 |
| NS@PEG | NA | 195 | −5.4 |
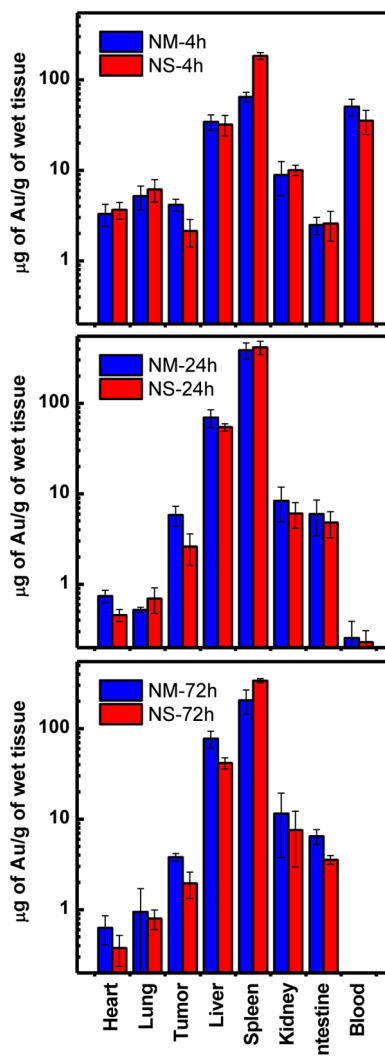


**Figure 3. Biodistribution of gold NM and NS in tumor-bearing mice.** Mean and standard deviation of gold content in organs at 4 h (top), 24 h (middle), and 72 h (bottom) after intravenous injection. Gold concentrations were analyzed by ICP-MS. The gold content in tumors in $\mu$g of Au/g of wet tissue is plotted as log$_{10}$ scale for visual clarity of values in organs with low gold content.

a circulation half-life of 12.7 h.[34] The gold concentration in the blood at 4 h is high, suggesting that the nanoparticles are still actively circulating in the bloodstream. Therefore, we can see that highly irrigated organs within the bloodstream (e.g., lung and heart) show a correspondingly high Au content at 4 h. A nontrivial concentration of Au was observed in kidney that is in line with what has been observed previously in several

studies using nanoshells.[34,35] It is thought that the presence of larger nanoparticles in the kidneys is due to accumulation within and subsequent transport by phagocytotic cells.[36] At all time points, the mean Au content in tumor (given in $\mu$g of Au per g of tumor) is $\sim$1.7 times higher for nanomatryoshkas than for nanoshells, presumably because the smaller size of nanomatryoshkas facilitates better penetration into tissue. Considering that the mass of Au in a single nanomatryoshka is $5.22 \times 10^{-9} \mu$g and in a nanoshell is $1.62 \times 10^{-8} \mu$g, the number of nanoparticles in the tumor was calculated; results are shown in Figure 4A. The percentage of the injected dose is also included in Figure 4B for comparison. As is clearly shown in Figure 4B, a larger percentage of the injected dose of NM is present in the tumor compared to NS at each of the time points.

The presence of the Au nanoparticles in the tumor was visualized by dark field microscopy due to the nanoparticle light scattering combined with fluorescence staining of cancer cells (Figure 4C). DAPI stains the cell nuclei blue; Alexa Fluor594 in combination with CD34 stains the vasculature red; and light scattering from nanoparticles is observed as yellow bright spots. Qualitatively in these images, more Au nanomatryoshkas are observed than nanoshells in the tumor tissue. Given the smaller scattering cross section of nanomatryoshkas, these images further support a greater degree of uptake in the tumor tissue by nanomatryoshkas relative to nanoshells

**Photothermal Therapy Efficacy.** Mice bearing 200 mm[3] triple negative breast tumors (MDA-MB-231-LM2) were randomly assigned to three experimental groups: (1) a control group treated with an injection of saline solution plus laser treatment (no nanoparticles) ($n = 4$), (2) nanoshell injection plus laser treatment ($n = 6$), and (3) nanomatryoshka injection plus laser treatment ($n = 6$). Mice received, *via* tail vein injection, a volume of 200 $\mu$L of PEG conjugated nanomatryoshkas or nanoshells at equal Au dose (300 $\mu$g of Au), equivalent to $5.7 \times 10^{10}$ nanomatryoshkas and $1.9 \times 10^{10}$ nanoshells. Laser photothermal ablation of TNBC tumors was conducted 4 h after injection. Laser power was 2 W/cm^{2} for 5 min.

The temperature in the tumor was probed using a needle thermocouple while the treatment was conducted. After 5 min of laser treatment the average maximum temperature change in the tumor was $13.7 \pm 1.0$ °C for the "saline + laser" group, $31.1 \pm 0.7$ °C for the "nanoshell + laser" group, and $33.7 \pm 8.0$ °C for the "nanomatryoshka + laser" group. While a higher temperature for the "nanomatryoshka + laser" than the "nanoshell + laser" group was expected due to the higher number of nanomatryoshkas in the tumors, no statistical difference was observed. We attribute this to the high sensitivity of thermocouple-based measurements to probe placement in the tumor, which is extremely difficult to reliably reproduce from mouse to mouse.
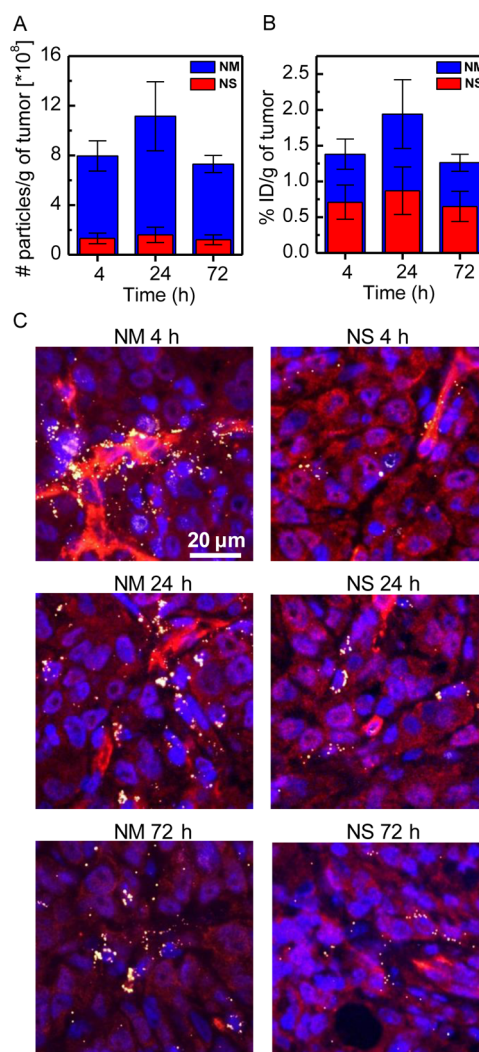


Figure 4. (A) Mean number of gold nanoparticles in the tumor per gram of wet tissue with standard deviations. The mass of gold in the tumors was analyzed by ICP-MS and converted to the number of nanoparticles considering the mass of Au in a nanomatryoshka = $5.22 \times 10^{-9} \mu$g for nanomatryoshka dimensions $[r_1, r_2, r_3]$ = [21, 31, 44] nm and for nanoshell = $1.62 \times 10^{-8} \mu$g of Au for a nanoshell with dimensions $[r_1, r_2]$ = [62, 76] nm. (B) Mean percentage of the total injected Au dose (% ID/g of tumor). (C) Histology of tumor sections extracted from mice intravenously injected with gold nanoparticles. Fluorescence staining combined with dark field microscopy: DAPI stains cell nucleus in blue; Alexa Fluor594 in combination with CD34 stains vasculature in red; and nanoparticle scattering is observed as bright spots. The three channels (DAPI, Alexa Fluor594 and nanoparticle scattering) are overlaid (see individual channels in Supporting Information, Figure S1).

Tumor size and mice health was monitored for the subsequent 60 days post-treatment, and mice were sacrificed when tumor size exceeded 1500 mm[3], or after completion of the experiments if tumors persisted at 60 days after treatment. The survival curve for complete tumor regression (no tumor detectable by bioluminescence imaging, or otherwise palpable or visually noticeable) is shown in Figure 5. For nanomatryoshkas, a large percentage (83%) of the TNBC
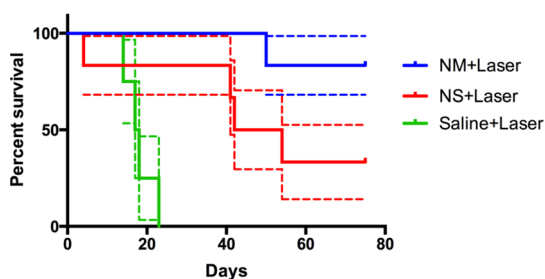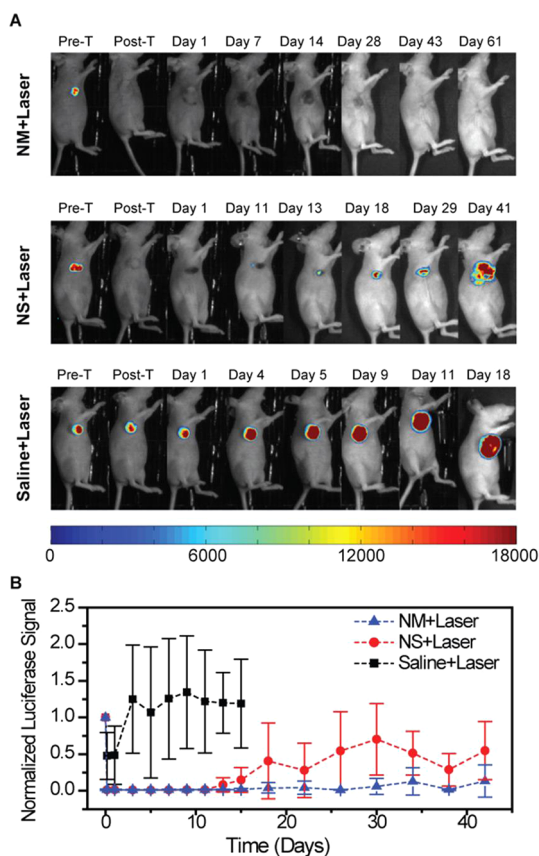
**Figure 5. Survival curves of tumor-bearing mice after photothermal therapy, which consisted of intravenous injection of gold nanoparticles or saline solution followed by irradiation for 5 min with a laser of wavelength at 810 nm and power of 2 W/cm². Bounds at 95% confidence intervals are drawn with dotted lines. The survival curves and trend differences were statistically significant ($p < 0.005$).**



**Figure 6. Evaluation of tumor response to photothermal therapy by bioluminescence imaging. The bioluminescence signal is generated only in living cancer cells as a result of luciferase activity. (A) Representative mice of each experimental group showing the luciferase activity in the tumor. The mice injected with nanomatryoshkas or nanoshells and treated with laser experienced loss of bioluminescence in the area illuminated by the laser as seen after therapy. Mice were euthanized when tumor volume reached 1500 mm³ or if the tumor persisted at 60 days after treatment. (B) Mean luciferase activity in the tumor with standard deviations. The luciferase signal was normalized to the signal before treatment.**

tumor-bearing mice appeared healthy and tumor free >60 days later, where only 33% of the nanoshell-treated mice survived the same period. One NS treated mice died within 4 days of treatment, likely due to thermal therapy off-target effects, as the tumors were close to liver, where nanoparticles preferentially accumulated. All animals in the control group had to be euthanized between 14 and 20 days post-treatment due to rapid tumor growth above animal protocol cutoff. The survival curves for the different treatment groups were compared with Logrank (Mantel−Cox) test with $p = 0.0008$, and Logrank test for trends ($p = 0.0006$), and also with Gehan−Breslow−Wilcoxon test with $p = 0.0025$. Analysis was performed with Prism software (Prism 6 for Mac OS X, GraphPad Software, La Jolla California USA, www.graphpad.com).

These results indicate that photothermal therapy using nanomatryoshkas improves the survival of mice bearing TNBC tumors compared to the equivalent therapy using nanoshells.

**Imaging of Luciferase Activity in Tumors.** Imaging of luciferase bioluminescence helps to evaluate the tumor response to the photothermal treatment (Figure 6). Bioluminescence signal intensity provides a surrogate measurement for cancer cell viability. Photothermal therapy resulted in a drastic loss of luciferase activity in mice injected with nanomatryoshkas or nanoshells. In contrast, mice injected with saline solution and treated with laser did not exhibit significant decrease in bioluminescent intensity thus reflecting a nonmeasurable therapeutic effect. In both experimental groups, "nanomatryoshka + laser" and "nanoshell + laser", the fraction of mice free of palpable or otherwise obvious tumors showed zero luciferase activity even after >60 days indicating complete eradication of cancer. However, one mouse in the "nanomatryoshka + laser" group and three in the "nanoshell + laser" group showed recurrence of luciferase activity and thus tumor relapse after intitial successful treatment. As depicted in Figure 6D, the

recurrence of luciferase activity took longer time for mice treated with nanomatryoshkas than with nanoshells and was lower in magnitude indicating persistent effects on nanomatryoshka therapy, even after tumor recurrence.

## CONCLUSIONS

Gold nanomatryoshkas exhibited improved photothermal therapy efficacy for orthotopic TNBC xenografts in nude mice when compared to standard gold nanoshells. We have demonstrated that nanomatryoshkas are highly efficient photothermal transducers due to their large absorption cross sections. The photothermal transduction efficiency of nanomatryoshkas was 63 versus 39% for nanoshells. In addition, the tumor uptake of nanomatryoshkas was 5 times the number of nanoshells when both particle types were injected at equal doses of Au mass. This higher tumor uptake was due to the smaller size of the nanomatryoshkas

(∼90 nm diameter) compared to nanoshells (∼150 nm diameter). These sub-100 nm gold nanomatryoshkas are promising NIR photothermal transducers for the treatment of highly aggressive tumors.

## METHODS

Synthesis of gold nanoshells was conducted by standard methods described in detail elsewhere.[11,29]

**Gold Nanomatryoshka Synthesis.** Gold nanomatryoshkas were synthesized by improving our previously reported method.[7]

*Synthesis of Silica Coated Gold Colloid.* Au colloid (40 nm citrate NanoXact Gold, nanoComposix) was coated with silica doped with (3-aminopropyl)triethoxysilane (APTES) by a modified Stöber process. For this reaction, 21 mL of Au colloid (7.0 × 10$^{10}$ particles/mL, citrate-capped 40 nm Au sphere, NanoComposix) were added under stirring to an Erlenmeyer flask with a ground glass joint. Next, 180 mL of 200 proof ethanol (Decon Laboratories), and 1.8 mL of ammonium hydroxide (28–30%, EMD Chemicals) were added. Finally, 36 μL of a solution of 10% tetraethoxysilane (TEOS, SIT7110.2, Gelest) in ethanol and 36 μL of 10% APTES (SIA0610.1, Gelest) in ethanol were added. The solution was sealed and stirred 50 min at room temperature followed by stirring 24 h at 4 °C. The solution was transferred into a dialysis membrane (Spectra/Por 6, MWCO = 10000, Spectrum Laboratories) previously washed with Milli-Q grade water to remove residual chemicals and then washed with ethanol to remove excess water. The solution was then dialyzed at least 12 h in 1 gallon of 200 proof ethanol at room temperature to remove ammonium hydroxide and the remaining free silanes (TEOS and APTES) from the reaction. The purpose of the dialysis is to decrease aggregation of nanoparticles during centrifugation. The solution was cooled to 4 °C and centrifuged 45 min at 2000 rcf (the solution was centrifuged in aliquots of ∼17 mL using 50 mL plastic tubes). The supernatant was removed and the pellet was redispersed by sonication in a total volume of 5 mL of ethanol. If there is red color in the supernatant, we repeated centrifugation to recover more particles.

*Synthesis of Duff Colloid.* Briefly, under rapid stirring, 1.2 mL of 1 M NaOH were added to 180 mL of H$_2$O, followed by addition of 4 mL of a 1.2 mM aqueous tetrakis(hydroxymethyl) phosphonium chloride (THPC, 80% solution in H$_2$O, Sigma). After stirring 5 min, 6.75 mL of 1% (w/v) aqueous chloroauric acid (HAuCl$_4$·3H$_2$O, Sigma-Aldrich) were quickly added, after which the solution immediately turned brown. The final solution was refrigerated for at least 2 weeks before use.

*Synthesis of Seeded Precursor.* The fabrication of the seeded precursor consists of the functionalization of APTES-doped silica surface with small gold colloid (1–2 nm) fabricated by the method reported by Duff et al.[28] First, the APTES-doped silica-coated gold colloids were bath sonicated for 20 min. Then, in a 50 mL plastic centrifuge tube, 20 mL of Duff colloid solution was added, followed by rapid, simultaneous addition of 300 μL of 1 M NaCl and 1 mL of APTES-doped silica-coated gold colloid (this reaction is repeated until we use all the silica-coated gold colloids, usually ∼4 reactions per batch). The solution was quickly vortexed and sonicated for 30 min. The resulting solutions were incubated 4 days at room temperature and gently shaken once at day followed by sonication 20 min to prevent aggregation. During this time two processes took place: (1) the silica was etched and (2) small gold colloids were attached to the surface of the silica-coated gold colloid. After the incubation, the solutions were sonicated for 20 min and then centrifuged 30 min at 700 rcf. The supernatant was transferred into a new tube, and the pellet was redispersed in 800 μL of water by sonication 5 min and transferred into a 2 mL centrifuge tube. We repeated the centrifugation of the supernatant and recovery of pellets three times (in total about 16 pellets were collected, each one distributed separately in 2 mL tubes). All solutions were centrifuged in the 2 mL tubes 30 min at 700 rcf and redispersed in water by sonication 5 min. Centrifugation was repeated but particles were redispersed and combined in a total volume of ∼1 mL of water.

This particle is the seeded precursor used for seeded growth of the outer Au shell.

The synthesis of a metallic shell of gold around the seeded precursor was done using a plating solution as a source of Au$^{3+}$. The plating solution was prepared by mixing 200 mL of water, 50 mg of anhydrous potassium carbonate (K$_2$CO$_3$), and 3 mL of 1 wt % aqueous chloroauric gold solution followed by aging for 12–19 h. The reduction of Au$^{3+}$ into a metallic shell of Au around the seeded precursor was done in a 4.5 mL metacrylate cuvette with a plastic cap. A volume of 3 mL of plating solution was added into the cuvette followed by 20–60 μL of seeded precursor. Next, 15 μL of formaldehyde were dropped inside the cap, and the cuvette was closed followed by a fast shaking of the solution for about 1 min. The solution changed color from red to purple upon the formation of the outer shell. The extinction spectra of gold nanomatryoshkas were measured in a UV–vis–NIR spectrophotometer (Cary 5000, Varian). The plasmon resonance of the nanomatryoshka was controlled by altering the volume of seeded precursor in the reaction. The concentration of nanomatryoshkas as synthesized is ∼9 × 10$^9$ particles/mL.

**PEG Conjugation to Nanoparticles.** Freshly made nanoparticles were centrifuged, nanoshells (∼300 mL of ∼3 × 10$^9$ parts/mL) at 240 rcf for 30 min and nanomatryoshkas (∼100 mL of ∼9 × 10$^9$ parts/mL) at 200 rcf for 30 min. Nanoparticles were redispersed in 10 mL of Milli-Q water. Thiol-PEG (mPEG-SH, MW 10000, Laysan Bio) was added to the nanoparticle solution to a final concentration of 100 μM and stirred for 12 h. Nanoparticle solutions were filtered through 0.8/0.2 μm pore size syringe filters (PALL Acrodisc PF 32 mm) to sterilize the solution. Finally, nanoparticle solutions were centrifuged (nanoshells 280 rcf for 30 min and nanomatryoshkas 240 rcf for 30 min) and redispersed in 4 mL of sterile 1 mM phosphate buffer pH 7.3. The Au concentration in each sample was analyzed by ICP-MS and was adjusted to 1.5 mg of Au/mL.

**Scanning Electron Microscope (SEM) Imaging.** First, silicon wafers (P-type/boron-doped silicon, Silicon Valley Microelectronics) were functionalized with PVP (poly(4-vinylpyridine), Sigma-Aldrich) by immersion in 1% (w/v) ethanolic solution for 24 h. Silicon wafers were washed with ethanol to remove excess PVP on the surface. Wafers were dried in a stream of nitrogen gas, and the sample of gold nanoparticles was drop-cast onto the silicon wafer and allowed to interact with the substrate for 1–4 h. The remaining solution was removed in a water rinse and the sample again dried with nitrogen. SEM imaging was performed using a Quanta 650 FEG SEM (FEI, Inc.). Nanoparticle dimensions were determined from SEM images with a custom MATLAB sizing program based on edge detection with a Hough transform.

**Photothermal Transduction Efficiency.** To measure the photothermal transduction efficiency, the nanoparticle solution was maintained under magnetic stirring in a 1 cm path length quartz cuvette that was clamped to a foam cap to reduce the heat loss. A K-type thermocouple connected to a digital thermometer (OMEGA, HH309A) was inserted through the foam cap to measure the temperature of the solution. The bottom of the cuvette was kept 1 cm above the magnetic stir plate and 1 cm separated from the continuous diode laser (810 nm laser, Diomed). The probe of the thermocouple was carefully submerged into the solution and kept away from the illumination path of the laser light. The solution was irradiated with 2 W/cm$^2$.

**Triple Negative Breast Cancer Xenografts.** MDA-MB-231LM2 cells, transfected with luciferase, were maintained in DMEM media (Sigma), supplemented with 10% FBS (Gibco) and 1% penicillin and streptomycin (Lonza) and incubated in 5% CO$_2$ at 37 °C as described in literature.[37] Cells were routinely maintained by passaging when they became 80% confluent.

Prior to injection into the mice, the cells were collected with a sterile plastic scraper, counted and suspended in sterile PBS to the desired cell number concentration. Mice used in this experiment were 4−5 week old athymic nude mice from Harlan Sprague−Dawley. To induce tumor growth, $1 \times 10^7$ cells in a total volume of 200 $\mu$L of PBS were injected subcutaneously in the fat pack of the ribcage on one side following the method described by Rimawi et al.[38] Tumor growth was monitored every 2 days by measurement with a digital caliper and the tumor volume was calculated with the formula: tumor volume = 1/2 (length $\times$ width$^2$). All in vivo studies were conducted in accordance with institutional guidelines and under approved IACUC protocols at Baylor College of Medicine.

**Photothermal Therapy Efficacy Experiment.** When the tumors reached a volume of around ~200 mm$^3$, 200 $\mu$L of either PEG conjugated nanomatryoshkas (NM-PEG), PEG conjugated nanoshells (NS-PEG) or a saline solution were injected into the tail vein. The gold concentration in both nanoparticle solutions was 1.5 mg of Au/mL. Four hours after injection, the mice were anesthetized with isoflurane and the tumor in the treatment groups was treated for 5 min with a CW-diode laser (Diomed 15Plus, Angio Dynamics) emitting 2 W/cm$^2$ at a wavelength of 808 nm. Mouse were observed for 60 days and euthanized via $CO_2$ if tumor size exceeded 1500 mm$^3$, or if tumors persisted at 60 day after treatment.

**Biodistribution.** When tumors reached the same volume as used for the photothermal therapy treatment, 18 mice were randomly put into two groups with nine mice per group. One group was injected with NM-PEG and the other with NS-PEG. The injected dose was 200 $\mu$L of nanoparticle solution equal to 300 $\mu$g of Au. Four hours, 24 and 72 h after injection, three mice per group were sacrificed. Heart, lung, liver, spleen, gut, kidney, blood and tumor were collected, the organs were washed in PBS and stored at −80 °C until further investigation.

For the gold content analysis, the organs were weighed and digested in ~2 mL of aqua regia. The samples were purified and diluted in 10 mL 1% aqua regia for inductively coupled plasma mass spectrometry (ICP-MS, PerkinElmer) analysis. The experiments were carried out in three independent runs for statistical analysis.

**Histopathology.** Small tumor parts were washed in PBS, held in 10% buffered formalin for 24 h, washed in PBS (3$\times$ for 20 min) and then kept in 70% ethanol. For the staining, the organs were fixed in paraffin blocks and then cut with a microtome. Vasculature was stained with CD34 (LifeSpan Biosciences) and Alexa Fluor594 (Molecular Probes, InVitrogen) and the nucleus was stained with DAPI (Vector Laboratories). Dark field and fluorescence microscopy of tumor sections was conducted with an Olympus BX 41 microscope with a 40$\times$ NA0.6 objective.

**Calculation of Nanoparticle Concentration.** In order to calculate the nanoparticle concentration, the extinction efficiency ($Q_\varepsilon$) was determined for nanomatryoshkas and nanoshells using Mie theory.[39] For nanomatryoshkas, the theoretical parameters used were [$r_1$, $r_2$, $r_3$] = [21, 31, 46] nm, dielectric constant of the $SiO_2$ (3.0), dielectric constant of the medium ($H_2O$, 1.77), and dielectric constant of Au from Johnson and Christy,[40] and theoretical extinction efficiency ($Q_\varepsilon$, 5.53). The dielectric constant of $SiO_2$ (3.0) required to match the experimental spectrum was higher than pure silica (2.04), likely due to a combination of factors such as doping of APTES in the silica, attachment of dyes, and filling of small gold colloid in the cracks of the silica, which would lead to an effective medium with an elevated refractive index. For nanoshells, the parameters chosen were [$r_1$, $r_2$] = [62, 74] nm, dielectric constant of the $SiO_2$ (2.04), dielectric constant of the medium ($H_2O$, 1.77), and Johnson and Christy dielectric constant for Au, and theoretical extinction efficiency ($Q_\varepsilon$, 8.49). The Beer−Lambert law was used to determine the concentration of the nanoparticle as follows:

$$\frac{\text{particles}}{\text{mL}} = \frac{2.303 \times \text{Abs}}{Q_\varepsilon \times \pi \times r^2 \times L} \quad (6)$$

where Abs is the experimental absorbance, $r^2$ is the overall nanoparticle radius in centimeters, and $L$ is the optical cell path length ($L$ = 1 cm).

*Conflict of Interest:* The authors declare no competing financial interest.

*Supporting Information Available:* Nonoverlaid fluorescence and dark field microscopy channels of tumor sections in Figure S1. Tumor volumes of each mouse during the survival study in Figure S2. This material is available free of charge via the Internet at http://pubs.acs.org.

## REFERENCES AND NOTES

1. Hirsch, L. R.; Stafford, R. J.; Bankson, J. A.; Sershen, S. R.; Rivera, B.; Price, R. E.; Hazle, J. D.; Halas, N. J.; West, J. L. Nanoshell-Mediated Near-Infrared Thermal Therapy of Tumors under Magnetic Resonance Guidance. *Proc. Natl. Acad. Sci. U. S. A.* **2003**, *100*, 13549–13554.

2. O'Neal, D. P.; Hirsch, L. R.; Halas, N. J.; Payne, J. D.; West, J. L. Photo-Thermal Tumor Ablation in Mice Using Near Infrared-Absorbing Nanoparticles. *Cancer Lett.* **2004**, *209*, 171–176.

3. Loo, C.; Lowery, A.; Halas, N.; West, J.; Drezek, R. Immuno-targeted Nanoshells for Integrated Cancer Imaging and Therapy. *Nano Lett.* **2005**, *5*, 709–711.

4. Dickerson, E. B.; Dreaden, E. C.; Huang, X.; El-Sayed, I. H.; Chu, H.; Pushpanketh, S.; McDonald, J. F.; El-Sayed, M. A. Gold Nanorod Assisted Near-Infrared Plasmonic Photo-thermal Therapy (PPTT) of Squamous Cell Carcinoma in Mice. *Cancer Lett.* **2008**, *269*, 57–66.

5. Melancon, M. P.; Lu, W.; Yang, Z.; Zhang, R.; Cheng, Z.; Elliot, A. M.; Stafford, J.; Olson, T.; Zhang, J. Z.; Li, C. In Vitro and In Vivo Targeting of Hollow Gold Nanoshells Directed at Epidermal Growth Factor Receptor for Photothermal Ablation Therapy. *Mol. Cancer Ther.* **2008**, *7*, 1730–1739.

6. Moon, H. K.; Lee, S. H.; Choi, H. C. In Vivo Near-Infrared Mediated Tumor Destruction by Photothermal Effect of Carbon Nanotubes. *ACS Nano* **2009**, *3*, 3707–3713.

7. Bardhan, R.; Chen, W.; Bartels, M.; Perez-Torres, C.; Botero, M. F.; McAninch, R. W.; Contreras, A.; Schiff, R.; Pautler, R. G.; Halas, N. J.; et al. Tracking of Multimodal Therapeutic Nanocomplexes Targeting Breast Cancer In Vivo. *Nano Lett.* **2010**, *10*, 4920–4928.

8. Chen, J.; Glaus, C.; Laforest, R.; Zhang, Q.; Yang, M.; Gidding, M.; Welch, M. J.; Xia, Y. Gold Nanocages as Photothermal Transducers for Cancer Treatment. *Small* **2010**, *6*, 811–817.

9. Weissleder, R. A Clearer Vision for In Vivo Imaging. *Nat. Biotechnol.* **2001**, *19*, 316–317.

10. Bardhan, R.; Grady, N. K.; Cole, J. R.; Joshi, A.; Halas, N. J. Fluorescence Enhancement by Au Nanostructures: Nano-shells and Nanorods. *ACS Nano* **2009**, *3*, 744–752.

11. Oldenburg, S. J.; Averitt, R. D.; Westcott, S. L.; Halas, N. J. Nanoengineering of Optical Resonances. *Chem. Phys. Lett.* **1998**, *288*, 243–247.

12. Gad, S. C.; Sharp, K. L.; Montgomery, C.; Payne, J. D.; Goodrich, G. P. Evaluation of the Toxicity of Intravenous Delivery of Auroshell Particles (Gold−Silica Nanoshells). *Int. J. Toxicol.* **2012**, *31*, 584–594.

13. Gentili, D.; Ori, G.; Comes Franchini, M. Double Phase Transfer of Gold Nanorods for Surface Functionalization and Entrapment into PEG-Based Nanocarriers. *Chem. Commun.* **2009**, 5874–5876.

14. Leonov, A. P.; Zheng, J.; Clogston, J. D.; Stern, S. T.; Patri, A. K.; Wei, A. Detoxification of Gold Nanorods by Treatment with Polystyrenesulfonate. *ACS Nano* **2008**, *2*, 2481–2488.

15. Vigderman, L.; Manna, P.; Zubarev, E. R. Quantitative Replacement of Cetyl Trimethylammonium Bromide by Cationic Thiol Ligands on the Surface of Gold Nanorods and Their Extremely Large Uptake by Cancer Cells. *Angew. Chem., Int. Ed.* **2012**, *51*, 636–641.

16. Sun, Y. G.; Xia, Y. N. Shape-Controlled Synthesis of Gold and Silver Nanoparticles. *Science* **2002**, *298*, 2176–2179.

17. Goodman, A. M.; Cao, Y.; Urban, C.; Neumann, O.; Ayala-Orozco, C.; Knight, M. W.; Joshi, A.; Nordlander, P.; Halas, N. J. The Surprising *In Vivo* Instability of Near-IR-Absorbing Hollow Au–Ag Nanoshells. *ACS Nano* **2014**, *8*, 3222–3231.

18. Kwon, Y. M.; Xia, Z.; Glyn-Jones, S.; Beard, D.; Gill, H. S.; Murray, D. W. Dose-Dependent Cytotoxicity of Clinically Relevant Cobalt Nanoparticles and Ions on Macrophages *In Vitro*. *Biomed. Mater.* **2009**, 4.

19. AshaRani, P. V.; Mun, G. L. K.; Hande, M. P.; Valiyaveettil, S. Cytotoxicity and Genotoxicity of Silver Nanoparticles in Human Cells. *ACS Nano* **2009**, *3*, 279–290.

20. Sun, Y.; Xia, Y. Alloying and Dealloying Processes Involved in the Preparation of Metal Nanoshells through a Galvanic Replacement Reaction. *Nano Lett.* **2003**, *3*, 1569–1572.

21. Day, E.; Thompson, P.; Zhang, L.; Lewinski, N.; Ahmed, N.; Drezek, R.; Blaney, S.; West, J. Nanoshell-Mediated Photo-thermal Therapy Improves Survival in a Murine Glioma Model. *J. Neurooncol.* **2011**, *104*, 55–63.

22. Pannerec-Varna, M.; Ratajczak, P.; Bousquet, G.; Ferreira, I.; Leboeuf, C.; Boisgard, R.; Gapihan, G.; Verine, J.; Palpant, B.; Bossy, E.; *et al. In Vivo* Uptake and Cellular Distribution of Gold Nanoshells in a Preclinical Model of Xenografted Human Renal Cancer. *Gold Bull.* **2013**, *46*, 257–265.

23. Dent, R.; Trudeau, M.; Pritchard, K. I.; Hanna, W. M.; Kahn, H. K.; Sawka, C. A.; Lickley, L. A.; Rawlinson, E.; Sun, P.; Narod, S. A. Triple-Negative Breast Cancer: Clinical Features and Patterns of Recurrence. *Clin. Cancer Res.* **2007**, *13*, 4429–4434.

24. Bauer, K. R.; Brown, M.; Cress, R. D.; Parise, C. A.; Caggiano, V. Descriptive Analysis of Estrogen Receptor (ER)-Negative, Progesterone Receptor (PR)-Negative, and Her2-Negative Invasive Breast Cancer, the So-Called Triple-Negative Phenotype: A Population-Based Study from the California Cancer Registry. *Cancer* **2007**, *109*, 1721–1728.

25. Silver, D. P.; Richardson, A. L.; Eklund, A. C.; Wang, Z. C.; Szallasi, Z.; Li, Q.; Juul, N.; Leong, C. O.; Calogrias, D.; Buraimoh, A.; *et al.* Efficacy of Neoadjuvant Cisplatin in Triple-Negative Breast Cancer. *J. Clin. Oncol.* **2010**, *28*, 1145–1153.

26. Chauhan, V. P.; Stylianopoulos, T.; Martin, J. D.; PopoviA, Z.; Chen, O.; Kamoun, W. S.; Bawendi, M. G.; Fukumura, D.; Jain, R. K. Normalization of Tumour Blood Vessels Improves the Delivery of Nanomedicines in a Size-Dependent Manner. *Nat. Nanotechnol.* **2012**, *7*, 383–388.

27. Wong, C.; Stylianopoulos, T.; Cui, J.; Martin, J.; Chauhan, V. P.; Jiang, W.; Popović, Z.; Jain, R. K.; Bawendi, M. G.; Fukumura, D. Multistage Nanoparticle Delivery System for Deep Penetration into Tumor Tissue. *Proc. Natl. Acad. Sci. U. S. A.* **2011**, *108*, 2426–2431.

28. Duff, D. G.; Baiker, A.; Edwards, P. P. A New Hydrosol of Gold Clusters. 1. Formation and Particle Size Variation. *Langmuir* **1993**, *9*, 2301–2309.

29. Brinson, B. E.; Lassiter, J. B.; Levin, C. S.; Bardhan, R.; Mirin, N.; Halas, N. J. Nanoshells Made Easy: Improving Au Layer Growth on Nanoparticle Surfaces. *Langmuir* **2008**, *24*, 14166–14171.

30. Roper, D. K.; Ahn, W.; Hoepfner, M. Microscale Heat Transfer Transduced by Surface Plasmon Resonant Gold Nanoparticles. *J. Phys. Chem. C* **2007**, *111*, 3636–3641.

31. Pattani, V. P.; Tunnell, J. W. Nanoparticle-Mediated Photothermal Therapy: A Comparative Study of Heating for Different Particle Types. *Laser Surg. Med.* **2012**, *44*, 675–684.

32. Arvizo, R. R.; Miranda, O. R.; Moyano, D. F.; Walden, C. A.; Giri, K.; Bhattacharya, R.; Robertson, J. D.; Rotello, V. M.; Reid, J. M.; Mukherjee, P. Modulating Pharmacokinetics, Tumor Uptake and Biodistribution by Engineered Nanoparticles. *PLoS One* **2011**, 6.

33. Lipka, J.; Semmler-Behnke, M.; Sperling, R. A.; Wenk, A.; Takenaka, S.; Schleh, C.; Kissel, T.; Parak, W. J.; Kreyling, W. G. Biodistribution of PEG-Modified Gold Nanoparticles Following Intratracheal Instillation and Intravenous Injection. *Biomaterials* **2010**, *31*, 6574–6581.

34. Xie, H.; Wang, Z. J.; Bao, A.; Goins, B.; Phillips, W. T. *In Vivo* PET Imaging and Biodistribution of Radiolabeled Gold Nanoshells in Rats with Tumor Xenografts. *Int. J. Pharm.* **2010**, *395*, 324–330.

35. James, W. D.; Hirsch, L. R.; West, J. L.; O'Neal, P. D.; Payne, J. D. Application of INAA to the Build-up and Clearance of Gold Nanoshells in Clinical Studies in Mice. *J. Radioanal. Nucl. Chem.* **2007**, *271*, 455–459.

36. Choi, C. H. J.; Zuckerman, J. E.; Webster, P.; Davis, M. E. Targeting Kidney Mesangium by Nanoparticles of Defined Size. *Proc. Natl. Acad. Sci. U. S. A.* **2011**, *108*, 6656–6661.

37. Minn, A. J.; Gupta, G. P.; Siegel, P. M.; Bos, P. D.; Shu, W.; Giri, D. D.; Viale, A.; Olshen, A. B.; Gerald, W. L.; Massague, J. Genes That Mediate Breast Cancer Metastasis to Lung. *Nature* **2005**, *436*, 518–24.

38. Rimawi, M. F.; Wiechmann, L. S.; Wang, Y. C.; Huang, C.; Migliaccio, I.; Wu, M. F.; Gutierrez, C.; Hilsenbeck, S. G.; Arpino, G.; Massarweh, S.; *et al.* Reduced Dose and Intermittent Treatment with Lapatinib and Trastuzumab for Potent Blockade of the Her Pathway in Her2/Neu-Overexpressing Breast Tumor Xenografts. *Clin. Cancer Res.* **2011**, *17*, 1351–61.

39. Mie, G. Beiträge Zur Optik Trüber Medien, Speziell Kolloidaler Metallösungen. *Ann. Phys.* **1908**, *330*, 377–445.

40. Johnson, P. B.; Christy, R. W. Optical Constants of the Noble Metals. *Phys. Rev. B: Solid State* **1972**, *6*, 4370–4379.